Tikrit Journal of Engineering Sciences (2025); 32(Sp1): 2737
DOI: http://doi.org/10.25130/tjes.sp1.2025.10

IRAQI Academic Scientific Journals

ISSN: 1813-162X (Print); 2312-7589 (Online)
Tikrit Journal of Engineering Sciences
available online at: http://www.tj-es.com

TJES Tikrit Journal of Engineering Sciences

Application of Deep Learning and IoT for Detection of Diabetic Retinopathy and Diabetic Macular Edema

Sanjaya Kumar Jena [a], Debahuti Mishra [a], Binod Kumar Pattanayak [*a], Pravat Kumar Rautaray [a], Bibhuti Bhusan Dash [b]

a Department of Computer Science & Engineering, Institute of Technical Education and Research, Siksha 'O' Anusandhan, Deemed to be University, Bhubaneswar, Odisha, India.
b School of Computer Application, Kalinga Institute of Industrial Technology (KIIT) Deemed to be University, Bhubaneswar, Odisha, India.

Keywords:
Diabetic Retinopathy (DR); Internet of Things (IoT); Convolutional Neural Networks (CNN); Diabetic Macular Edema (DME).

Highlights:

- IoT-based Deep Learning for DR and DME detection.
- Proposed Multi-Level Feature Extraction and Classification (ML-FEC) deep learning architecture.
- ML-FEC achieved 98.86% accuracy for DME and 86.04% for DR.
- Homomorphic Encryption used to secure medical images/diagnosis.
- Model uses ResNet50 transfer learning on augmented Messidor-2 dataset.

ARTICLE INFO

Article history:

Received	02 Sep.	2025
Received in revised form	15 Sep.	2025
Accepted	14 Oct.	2025
Final Proofreading	25 Oct.	2025
Available online	27 Dec.	2025

Citation: Jena SK, Mishra D, Pattanayak BK, Rautaray PK, Dash BB. **Application of Deep Learning and IoT for Detection of Diabetic Retinopathy and Diabetic Macular Edema**. *Tikrit Journal of Engineering Sciences* 2025; **32**(Sp1): 2737.
http://doi.org/10.25130/tjes.sp1.2025.10

*Corresponding author:
Binod Kumar Pattanayak
Department of Computer Science & Engineering, Institute of Technical Education and Research, Siksha 'O' Anusandhan, Deemed to be University, Bhubaneswar, Odisha, India.

Abstract: In recent years, diabetes mellitus has been increasing rapidly, and due to that, around 380 million people around the globe have been affected. This disease may cause many people to become blind and other health issues. Diabetic Macular Edema (DME) and Diabetic Retinopathy (DR) are medical conditions in humans caused by prolonged high blood sugar levels and have a direct impact on human eyesight, which can subsequently lead to blindness. In the early stages, DR usually progresses without any remarkable symptoms, making early detection difficult. If left untreated for a prolonged period, it can result in permanent vision loss. To facilitate proper diagnosis and timely treatment, computer-based systems today often rely on clinical images. In fact, a vital indicator of DR is the presence of microaneurysms (MA), which are critical for identifying the onset of the disease. In line with the emergence of the Internet of Things (IoT), a wide range of electronic devices can be usefully interconnected and are very capable of collecting, transmitting, and responding to data in real time. In the field of human healthcare, such IoT-powered systems possess sufficient capabilities to support remote diagnosis, particularly through the use of medical sensors in telemedicine scenarios. Nonetheless, such a shift can lead to critical privacy issues for a patient. The protection of critical health-related information becomes particularly critical. Hence, the major challenge here is implementing remote systems to support remote diagnosis while ensuring strict confidentiality to protect the patient's privacy. In the present research work, an IoT-based deep learning approach achieving 98.86% accuracy for Diabetic Macular Edema (DME) and 86.04% for Diabetic Retinopathy is proposed.

1.INTRODUCTION

In the last two decades or so, data on diabetes published by global health organizations have significantly increased, leading to serious concerns for public health. As claimed by the IDF Diabetes Atlas, almost 500 million people have been diagnosed with diabetes globally across all age groups. Health professionals estimate this number may reach 700 million by 2045, underscoring a growing public health crisis. In addition, the Atlas predicts that by 2040, DR may presumably leave an impact on almost one in three people suffering from diabetes, a complication that arises from impairment of the retina's rear blood vessels. In the absence of a timely diagnosis and appropriate treatment, DR can progress and lead to significant vision impairment or even blindness, underscoring the critical necessity for early detection and prompt medical intervention [1]. Recently, the DR assessment has primarily relied on manual analysis of fundus images by healthcare professionals. This method is highly time-consuming and limited by a shortage of specialized personnel, particularly as the diabetic population grows. Consequently, a large number of diabetic patients fail to get in-time diagnoses, and consequently, the disease remains unnoticed till the moment it progresses to a severe stage. However, although routine retinal screenings are strongly recommended for people with diabetes, a significant number of such cases stay undetected until significant damage has occurred. Such a scenario underscores the urgent need for an automated system capable of efficiently identifying DR at an earlier stage, enabling timely care to improve patient outcomes [2]. Various studies in this field report using fundus images that provide a visual representation of the retina's current health status. By assisting with many procedures, such as DR detection, retinal blood vessel segmentation, and associated lesion identification, these pictures are necessary for DR diagnosis [3]. DR can be successfully detected and its progression monitored by identifying and classifying lesions in such fundus images. Microaneurysms (MAs), superficial retinal hemorrhages (SRHs), exudates (soft exudates (Ses)), cotton wool spots (CWSs), and intrareticular hemorrhages (IHEs) are the primary indicators. A comparison of retinas with and without DR is shown in Fig. 1, highlighting the diagnostic utility of these lesions in assessing the severity of the ailment. In addition, Figure 2 depicts the various phases of retinopathy. Such strategies significantly benefit from extensive labeled fundus image collections to train models sufficiently capable of accurately detecting and categorizing lesions linked to DR, including microaneurysms, hemorrhages, and exudates. By examining sufficiently complex features and patterns in the said images, machine learning algorithms are sufficiently capable of differentiating between retinas in good health and those that are not, while assessing the severity of the impairment. Deep learning is a subset of machine learning. It can significantly improve the accuracy of classification systems for DR, thereby enabling models to automatically learn hierarchical features directly from unprocessed image data. In deep learning, convolutional neural networks (CNNs) are a popular architecture that is convincingly effective for image recognition and has been successfully implemented for the detection and grading of DR. The accuracy and speed of diagnosing retinal illnesses have significantly improved with the implementation of AI technologies, particularly deep learning and machine learning. This advancement enables early detection and timely treatment of patients with diabetes, which is essential for preventing visual loss. Detection and grading are two major approaches to diagnosing DR. The strategy of binary classification that distinguishes between a retina in good health and one affected by DR is called detection. Grading, on the contrary, enables the identification and grading of affected retinal regions, thereby categorizing disease severity as mild, moderate, or severe [4]. These approaches are critical for accurate assessment of DR severity, which assists in planning necessary treatment and patient care [18]. Given the sensitivity of health-related information and the potential for modification and illegal access, security appears essential for medical image processing. To protect sensitive information, several crucial measures must be taken, with data encryption as the most vital strategy. Encryption of medical images during both storage and transmission ensures that the relevant information is accessible only to personnel with the correct decryption key. This study proposes using Homomorphic Encryption, i.e., a highly secure encryption method, to empower the protection of medical images [5].

1.1.Homomorphic Encryption

It is possible to perform the necessary calculations directly on the encrypted data received, without first decrypting it, using a cryptographic technique known as homomorphic encryption. The capabilities of such an encryption technique reveal that users can securely process and analyze sensitive information, thereby maintaining the confidentiality of the received information. In fact, the homomorphic encryption technique can transform data into a coded form, enabling analysis without revealing the underlying private information. To ensure the safe

encryption and decryption of the data, there are three basic forms of homomorphic encryption, each based on a public-key encryption technique. In real-world scenarios, homomorphic encryption enables splitting encrypted data into multiple segments, with a master key used to decrypt the entire dataset and additional keys to access specific portions. This feature allows multiple users to independently access and process different portions of the encrypted data. As a result, more precise control over data privacy can be achieved, thereby improving both security and confidentiality of the data [7]. Such an encryption has a few drawbacks as well, especially when the ciphertext becomes unnecessarily noisy, which may obstruct accurate decoding and trustworthy computation. The computational load herein increases linearly with noise levels, resulting in decreased performance and a seemingly slower encryption process. In a slightly homomorphic encryption (SHE) approach, the maximum number of successive multiplications, referred to as the multiplicative depth, may necessarily be limited to maintain reliability, which is another vital constraint. Despite such challenges, SHE remains a valuable tool, especially in physics-related fields where coherent states are involved. An instance of homomorphic encryption that can be fruitfully applied to medical imaging is presented in Figure 3. A list of different forms of homomorphic encryption is detailed below.

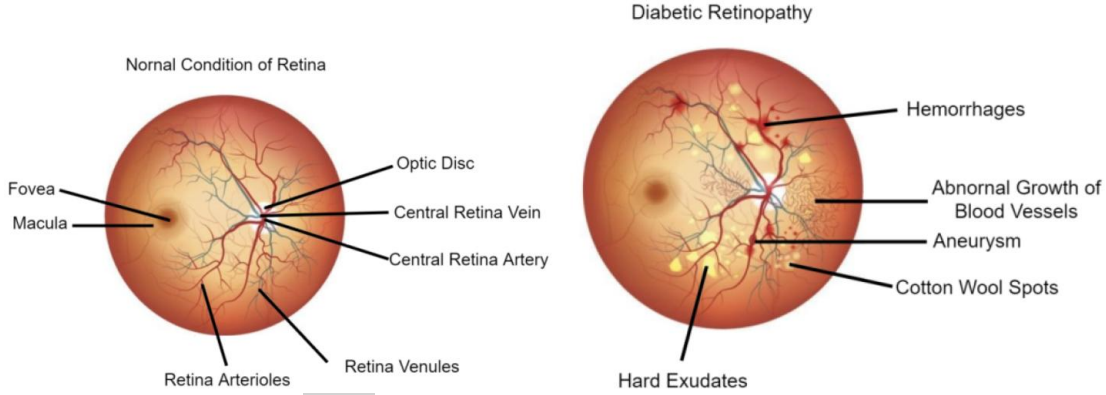

Fig. 1 Healthy Retina and Affected Retina.

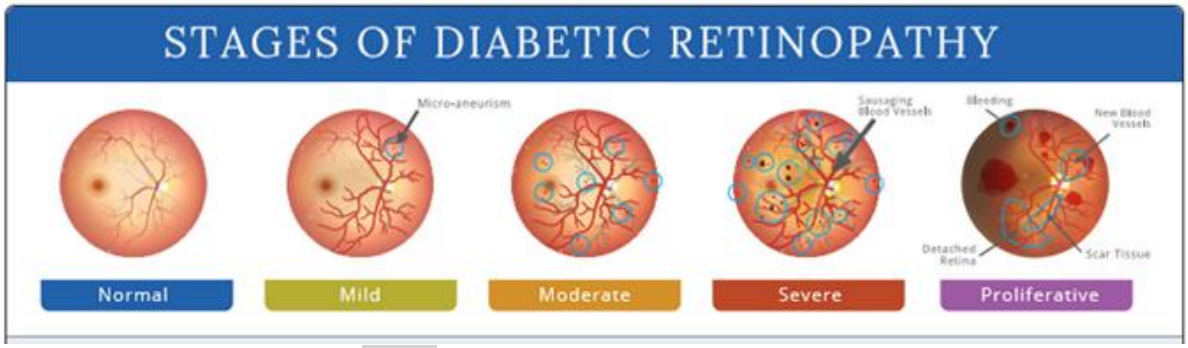

Fig. 2 Different Stages of Retinopathy.

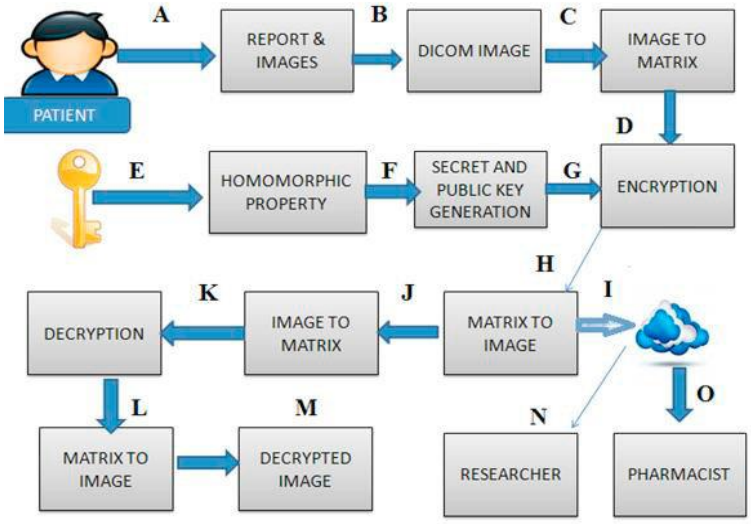

Fig. 3 Homomorphic Encryption: Encryption and Decryption.

1.2.Fully Homomorphic Encryption Vs Somewhat Encryption

Partial homomorphic encryption served as the basis for the development of fully homomorphic encryption. Although the mathematical concepts of the two types are identical, their capacities are very different. The main distinction is that partially homomorphic encryption has restrictions. Due to the noise accumulation in the ciphertext, it can only execute a limited number of mathematical operations on encrypted data. On the contrary, fully homomorphic encryption can overcome the aforementioned restrictions, thereby facilitating more complex computations over encrypted data [5]. Here, different encryption techniques serve different purposes and can be successfully applied in the same domain. For example, somewhat homomorphic encryption is more preferable for stationary 5G networks, wherein data paths are presumably limited and only a few processing units are involved in the process, whereas fully homomorphic encryption is comparatively more preferable for mobile 5G networks, for the reason that it necessarily supports more extensive homomorphic operations overcoming the bottlenecks induced from somewhat homomorphic encryption [6]. Fully Homomorphic Encryption (FHE) enables an unlimited number of operations on encrypted data, thereby facilitating addition and multiplication. On the other hand, Somewhat Homomorphic Encryption (SHE) supports limited operations that can eventually be performed, allowing only addition or multiplication, but not both at the same time, and often imposes restrictions on how many times these operations can be conducted. This significant distinction makes FHE more flexible for performing intricate, unbounded calculations on encrypted data. Among homomorphic encryption approaches, Fully Homomorphic Encryption (FHE) offers significantly greater flexibility and processing power. It consequently allows assessing any computational circuit, regardless of its depth, including those composed of different logic gates, such as AND, OR, and NOT. Because it can facilitate complex operations directly on encrypted data, avoiding decryption, FHE is beneficial for applications that require secure, private computation [7]. Fully Homomorphic Encryption (FHE) provides a robust approach to ensuring the security and privacy of data, particularly in challenging circumstances, such as high mobility, constrained bandwidth, and shifting network conditions. Its capability to perform complex computations directly on encrypted data makes it particularly effective in addressing the security demands of mobile networks, thereby strengthening data protection in these dynamic settings [8]. A description of homomorphic encryption is presented in Fig. 4.

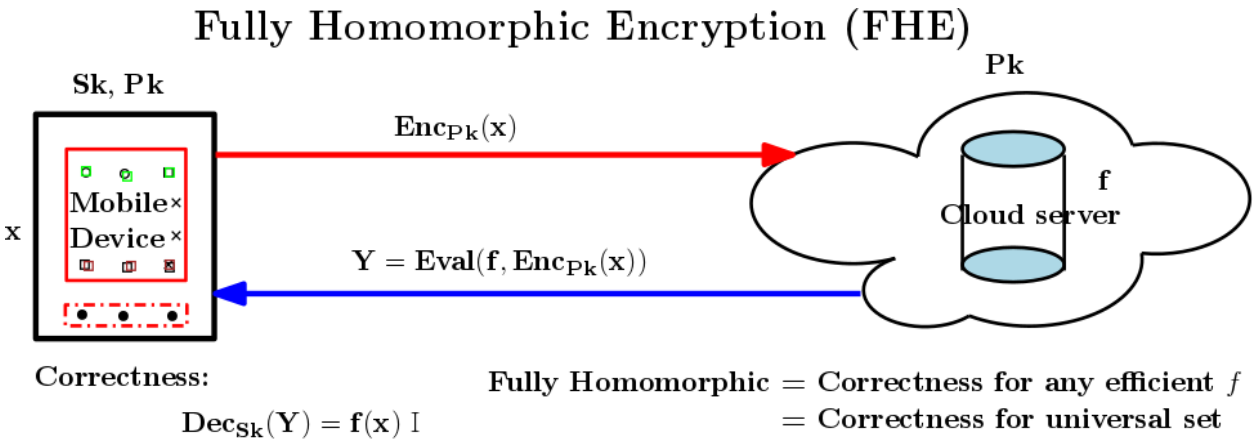

Fig. 4 Homomorphic Encryption.

1.3.Retina Dataset

The analysis of retina images for tasks such as blood vessel segmentation and DR detection is supported by numerous publicly available datasets. Such datasets are essential for benchmarking performance against similar systems and for training, validating, and testing various machine learning models. There are various approaches to retinal imaging, but the two most widely used are fundus photography and optical coherence tomography (OCT). It provides both 2D and 3D views of the retina using non-coherent light, offering detailed insights into its structure and thickness. However, fundus photography uses reflected light to create two-dimensional photographs of the retina. Recently, OCT has gained prominence due to its enhanced imaging capabilities. Furthermore, a variety of publicly available fundus imaging datasets are

frequently utilized in studies and the creation of diagnostic models [10]. Some of the most widely recognized fundus image datasets include:

- Eighty-nine retinal fundus images with a resolution of 1500 × 1152 pixels and a 50-degree field of view (FOV) comprise the publicly accessible dataset DIARETDB1 [9]. Of them, five depict healthy retinal states, and the remaining 84 depict cases of DR. Crucially, a team of four clinical specialists has meticulously examined and annotated every image in the collection to guarantee correct labeling and facilitate in-depth analysis.
- The Kaggle DR Dataset consists of 88,702 high-resolution retinal images with dimensions ranging from 433 × 289 pixels to 5184 × 3456 pixels, captured with various camera models. Five categories were used to arrange the dataset, each representing a different DR stage severity. While the whole dataset is available, detailed annotations are primarily provided for the training set, which is openly accessible. It is essential to be extremely cautious when dealing with this dataset, as some images may appear of inconsistent quality or may be incorrectly labeled.
- E-ophtha EX and E-ophtha MA are two distinguishable subsets of the E-ophtha retinal image dataset that are publicly available. The E-ophtha EX subset includes 35 retinal images without disease and 47 photos with exudates. Nevertheless, there are 148 photographs with microaneurysms and 233 images of healthy retinas in the E-ophtha MA subset. This organized division supports the targeted study of specific DR lesions.

A total of 13,673 retinal fundus images from 147 medical facilities spread across 23 Chinese regions are included in the Diabetic Retinopathy Dataset (DDR). The dataset is categorized into five groups based on the severity levels of diabetic retinopathy: no DR, mild DR, moderate DR, severe DR, and proliferative DR. An additional low-quality image category has been excluded from the dataset used in the present study. All images have been preprocessed to eliminate the black background for better analysis. Notably, 757 of these images have been carefully annotated to mark specific DR-related lesions, enabling lesion-level evaluation and model training.

The DRIVE (Digital Retinal Images for Vessel Extraction) dataset is currently publicly available for segmenting retinal blood vessels. It comprises 40 color fundus images, each with a field of view (FOV) of 45 degrees and a pixel size of 565 × 584. Seven of these images depict the early stages of mild diabetic retinopathy, whereas the others depict normal retinal characteristics. In retinal image analysis, datasets are most often used to evaluate vascular segmentation approaches. The High-Resolution Fundus (HRF) dataset has been developed for retinal blood vessel segmentation and comprises 45 images with a very high resolution, each with a resolution of 3504 × 2336 pixels. The dataset was split equally into three categories: 15 images of DR, 15 of healthy retinas, and 15 of glaucoma cases. Such an even distribution makes the HRF dataset viable for comparative analysis among multiple retinal pathologies.

1.4.MESSIDOR Dataset

Messidor Dataset is widely used, publicly accessible, supports research on DR, and is currently available in two main versions: Messidor-1 and Messidor-2. Such datasets have been designed to advance the development of computer-assisted diagnostic tools for DR. 1,200 color fundus images from Messidor-1 have a field of vision (FOV) of 45 degrees. Each image here has been carefully annotated to reflect various stages of diabetic retinopathy. Using RGB cameras, 800 images were obtained after pupil dilation and 400 without it, collected from three different ophthalmology centers. Macular edema risk has been split into three different groups: 1, 2, and 0 represent no, moderate, and high levels, respectively. In addition, each image has been labeled with diagnostic information, including DR severity stages split into four categories: mild (level 1), moderate (level 2), severe (level 3), and zero (no DR). Messidor-1 serves as a vital standard for assessing the effectiveness of automated systems for detecting and grading DR and identifying macular edema. Messidor-2 extends the original Messidor dataset by adding 1,748 retinal fundus images, also captured with a 45-degree FOV. This dataset comprises additional images gathered at Brest University Hospital in France, with 690 images taken at Brest between October 2009 and September 2010, and the remaining 1,058 images from the original Messidor dataset. Every picture was taken with a non-mydriatic fundus camera at a consistent 45° FOV, ensuring uniform image quality. The dataset is organized with a folder containing all image files and an associated CSV file that holds metadata, including 1,744 unique Image IDs and graded retinopathy diagnoses on a five-point scale: Grade 0 (1,017 images), Grade 1 (270 images), Grade 2 (347 images), Grade 3 (75 images), and Grade 4 (35 images). Additionally, diabetic macular edema (DME) is labeled as Grade 0 (no referable DME) for 1,593 images and Grade 1 (referable DME) for 151 images. The STARE dataset includes 20 retinal

images with a 35-degree field of view and a 700 × 605-pixel resolution intended for blood vessel segmentation. Ten of these photos display typical retinal architecture. The CHASE DB1 dataset is another publicly available collection for retinal blood vessel segmentation. It comprises 28 high-resolution images (1280 × 960 pixels) captured with a 30-degree field of view. With a 50-degree field of view (FOV), the Indian DR Image Dataset (IDRiD) has 516 fundus images. Each image is meticulously labeled to correspond to one of five DR stages. The ROC dataset includes 100 retinal images with a 45-degree field of view and sizes ranging from 768 × 576 to 1389 × 1383 pixels. Only the training set has ground-truth labels, even though every image is labeled for microaneurysms (MA) detection. Finally, the DR2 collection comprises 435 publicly available retinal images with a resolution of 857 × 569 pixels. Of the 98 photos identified as needing referral, each image includes annotations indicating whether additional clinical evaluation is necessary.

2.RELATED WORK

Using a Convolutional Neural Network (CNN), the Kaggle dataset's Images were classified as either normal or exhibiting DR symptoms. For the present investigation, 1,000 photos were taken from the dataset. Data augmentation techniques were applied to improve the dataset before importing the photos into the CNN model. The images were resized to 224×224×3 pixels. Augmentation methods such as rescaling, shearing, rotation, flipping, and translation were employed to increase the variety and volume of training data. The CNN architecture consisted of eight convolutional layers, four max-pooling layers, and two fully connected layers. The final classification layer used the SoftMax activation function to categorize each image. This approach achieved 94.5% accuracy in classifying images as referable or non-referable diabetic retinopathy using the model's predictions [11]. Additionally, the author suggested several pre-trained deep learning models for extracting and classifying multi-label features, specifically ResNet50, ResNet152, and SqueezeNet1, all of which use pre-trained CNN architectures. Experimental results demonstrated accuracies of 93.67% for ResNet50, 91.94% for SqueezeNet1, and 94.40% for ResNet152. These findings highlight the models' effectiveness and their potential for integration into routine clinical practice, supporting large-scale DR screening programs [12]. When the author recommended utilizing ResNet-3, a Gaussian filter, and image normalization, the model achieved 85% accuracy and 86% sensitivity in binary classification [13]. Using the ResNet50 model, the author achieved 92% sensitivity, 92.6% accuracy, and 96.3% area under the receiver operating characteristic (ROC) curve (AUC). The Messidor dataset and the ISBI 2018 IDRiD challenge dataset are two well-known benchmark datasets used to assess the network. The suggested method performed better than competing approaches in these evaluations. In the ISBI 2018 IDRiD competition, it performed best, demonstrating its strong ability to correctly classify photos of diabetic retinopathy. Additionally, it outperformed current techniques on the Messidor dataset, demonstrating its resilience and potency in DR detection. These findings, taken together, highlight the model's excellence and dependability in detecting DR from medical photos, as confirmed by extensive testing on recognized benchmark datasets [14]. Rautaray et al. [18] proposed a method achieving 95.1% accuracy in detecting macular edema via transfer learning with ResNet18.

3.METHODOLOGY

The present study introduces the detection of DR and DME using the Internet of Things (IoT) and the Multi-Level Feature Extraction and Classification (ML-FEC) architecture, a revolutionary deep learning architecture. Using IoT devices, the images were collected. Then, the images were forwarded to the cloud platform where the developed model is present. As shown in Fig. 5, the developed model is intended to identify and categorize DR lesions in color fundus photographs (CFPs) that cover all five stages of DR. Unlike traditional classification methods that treat output labels as mutually exclusive, the ML-FEC model adopts a multi-label classification strategy, enabling it to assign multiple relevant labels to a single image. This approach acknowledges the possibility of co-occurring lesions, enhancing diagnostic accuracy. By incorporating advanced deep learning methods in the framework of ML-FEC, the model significantly improves the precision and reliability of lesion detection and stage classification, accounting for the complex and varied presentations of DR. A distinctive advantage of the proposed method is its capacity to conduct a comprehensive analysis of CFPs by detecting multiple DR lesion types simultaneously, facilitating a deeper understanding of disease progression and supports more informed clinical decisions. The annotation process was conducted under expert oversight, with each image thoroughly reviewed and labeled by a team of specialists. The labels were documented in Excel spreadsheets and include diagnostic categories ranging from "No DR" to progressively severe stages, such as "Mild NPDR," "Moderate NPDR," "Severe NPDR," "Early PDR," and "High-risk PDR." Additionally, each image was annotated to highlight specific DR-associated lesion types. Figure 6 presents the systematic arrangement of the dataset, along with sample retinal images

that showcase distinct visual characteristics. These examples are accompanied by their respective classifications, as documented in the corresponding Excel annotation files. Here, a residual learning model has been proposed to train deep neural networks, improving the training of highly deep neural networks developed by Microsoft's research and development wing, called ResNet (Residual Network). In a traditional CNN, adding new layers can degrade performance due to vanishing gradients. Figure 7 illustrates the architectural implementation of Multi-Level Feature Extraction and Classification (ML-FEC). Here, from a single dataset, features are extracted to classify both classes: DR (5 classes) and DME (2 classes).

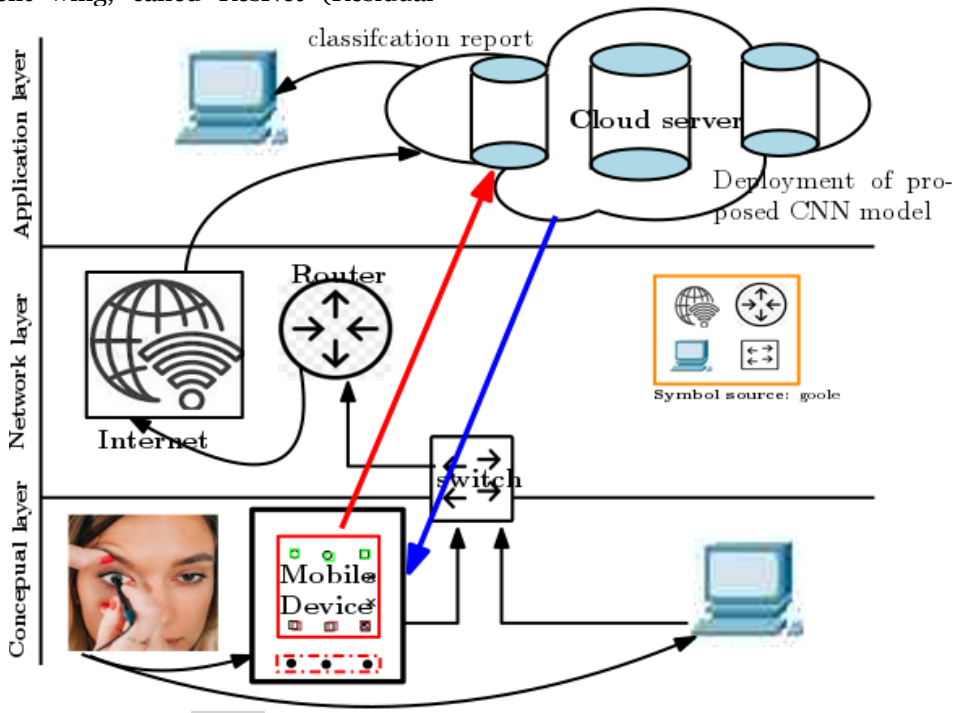

Fig. 5 Architecture of IoT Using a Mobile Device.

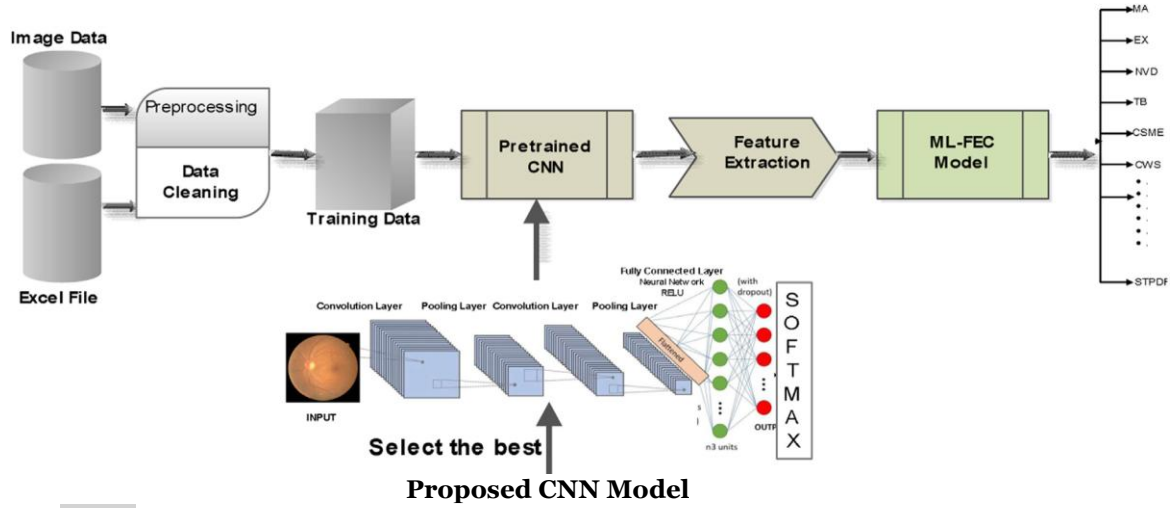

Fig. 6 Deep Learning Multi-Label Feature Extraction and Classification (ML-FEC) Model.

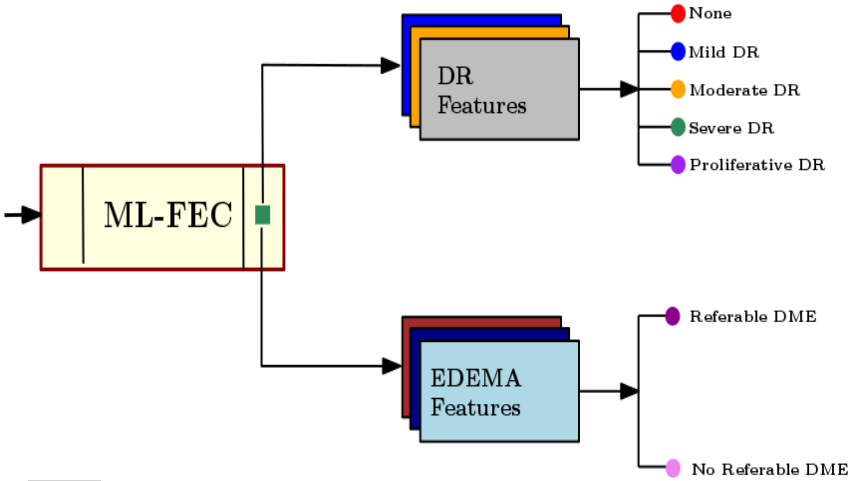

Fig. 7 Multi-Level Feature Extraction and Classification (ML-FEC).

In non-residual learning, the neural network learns directly from:

$$H(x) \quad (1)$$

where x is the input, and H(x) is the output mapping to be learned.

However, in residual learning, the neural network learns:

$$H(x)=F(x)+x \quad (2)$$

where F(x) is the residual function, and X is the input.

The architecture of the proposed residual learning is illustrated in Figure 8. Reusing a model trained on one job to address a different but related problem is known as transfer learning, and it is a crucial machine learning technique. Because of its strong performance and computational efficiency, ResNet (Residual Network) is one of the most widely used architectures in image classification. In particular, ResNet50 is a 50-layer deep convolutional neural network. A 7×7 convolutional filter was used in its first layer. The architecture was organized into four main convolutional stages, each consisting of two residual blocks. Each residual block had two learnable weighted layers and a skip link that adds the second layer's output straight to the activation function (ReLU). If the dimensions of the block's input and output matched, an identity shortcut was used. However, when they differed, a convolutional pooling layer adjusted the skip connection to match the shape. ResNet50 accepts input images with dimensions (224, 224, 3), where 3 denotes the number of RGB color channels, 224 the width, and 224 the height. The network ends with a fully connected (FC) layer that feeds into a sequential layer for final predictions. The use of residual connections in this architecture helps mitigate the vanishing gradient problem, making it easier to train deeper networks effectively. In this work, 2048 fully connected layers were used, with a new layer of size 512 connected from 512 to 128, then to 5 corresponding to the number of diabetic retinopathy classes. Similarly, for diabetic macular edema, the network will be 2048-512, 512-128, and 128-2, corresponding to the sizes of the edema classes. The architecture of the present CNN model is illustrated in Figure 9.

3.1.Experimental Setup Dataset

The present study used the Messidor-2 dataset, which includes a folder containing various diabetic retinopathy (DR) images and an accompanying CSV file with four columns. The dataset includes 1,744 unique image identifiers. These images were classified as 0: None (1,017 images),1: Mild DR (270 images),2: Moderate DR (347 images), 3: Severe DR (75 images), and 4: Proliferative DR (PDR) (35 images). A column for diabetic macular edema (DME) grading, classified as: 0: No Referable DME (1,593 images) and 1: Referable DME (151 images), as shown in Figure 10. Severe and proliferative DR were represented by only a few images, indicating an unbalanced dataset; therefore, it should be balanced by applying data augmentation.

3.2.Data Augmentation

Data augmentation plays a critical role, particularly in scenarios where labeled data is scarce. By generating modified versions of existing images, it increases the effective dataset size and enhances the model's ability to generalize to unseen data. In deep learning applications, this method is widely utilized, particularly when training convolutional neural networks (CNNs) for tasks such as object detection, image classification, and segmentation. In this study, augmentation methods applied to each image included horizontal and vertical flipping, rotation, grayscale conversion, Gaussian noise addition, channel shuffling, and Contrast Limited Adaptive Histogram Equalization (CLAHE). An example of an augmented image is illustrated in Figure 11. Since the task involves multilevel classification for both retinopathy and edema, the dataset was expanded and balanced using data augmentation. After augmentation, the distribution of retinopathy classes was as follows: "PDR": 335 photographs, "None":

1,017 images, "Mild DR": 318 images, "Moderate DR": 863 images, and "Severe DR": 777 images. The total number of retinopathy images was 3310. Figure 12 shows the distribution of the augmented dataset. The distribution of different dataset classes before and after DR augmentation is tabulated in Table 1, and the distribution of different DME classes is tabulated in Table 2.

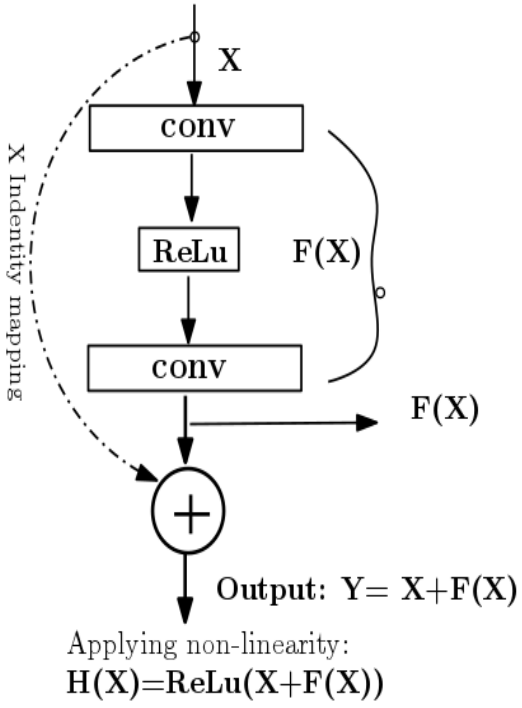

Fig. 8 Residual Learning.

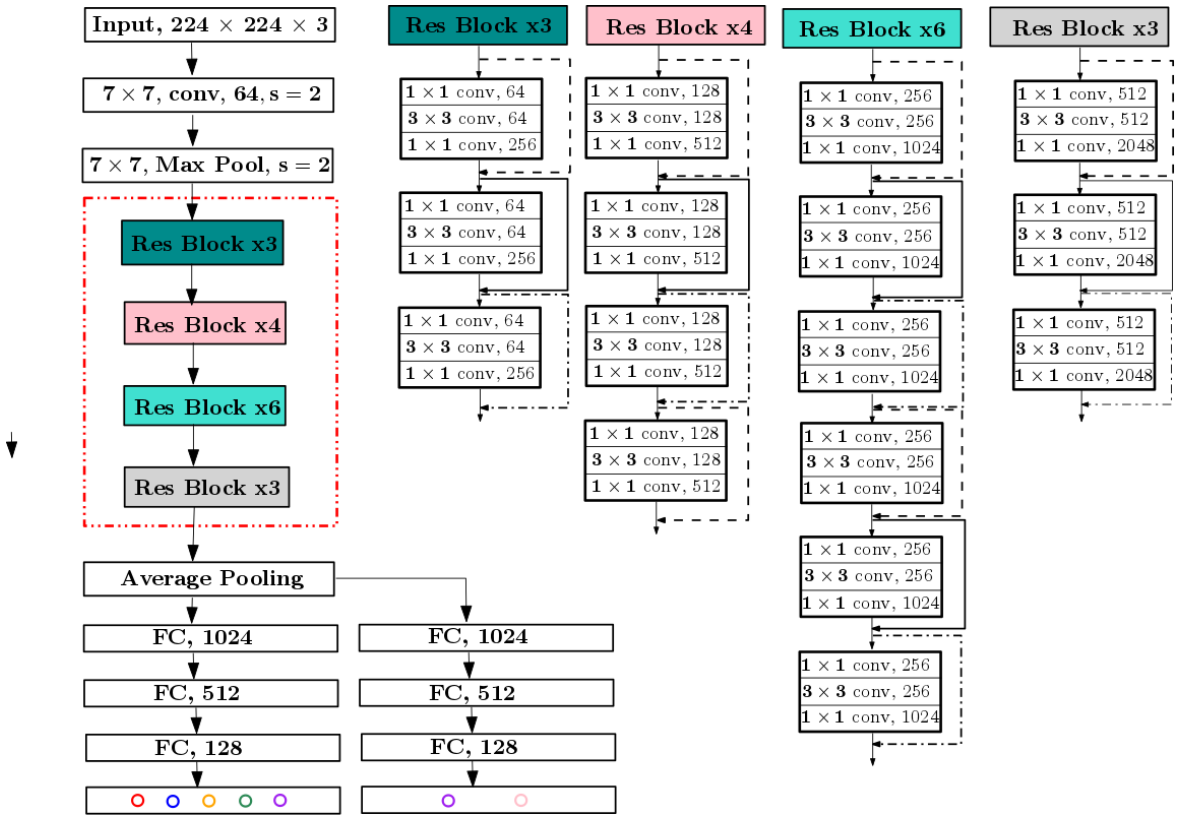

Fig. 9 Detailed Architecture of the Pretrained CNN Model for the Proposed Work.

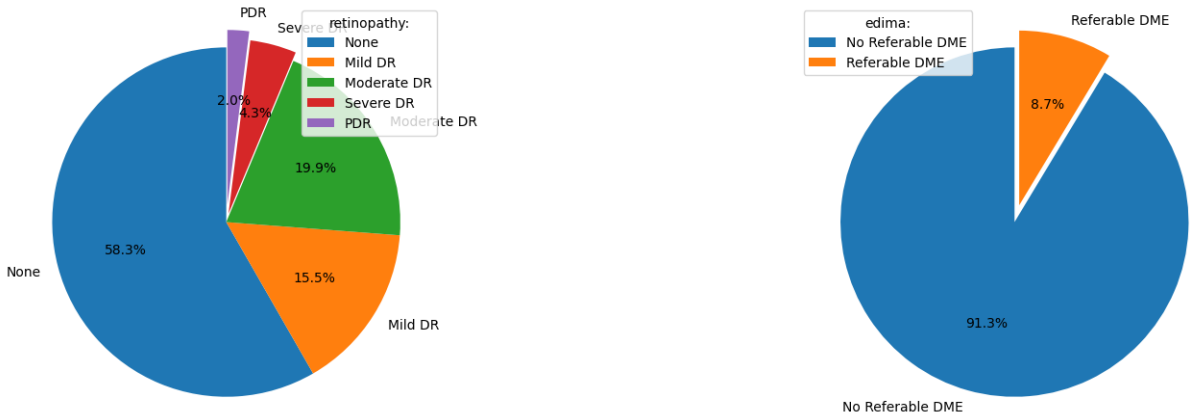

Fig. 10 Retinopathy and Edema.

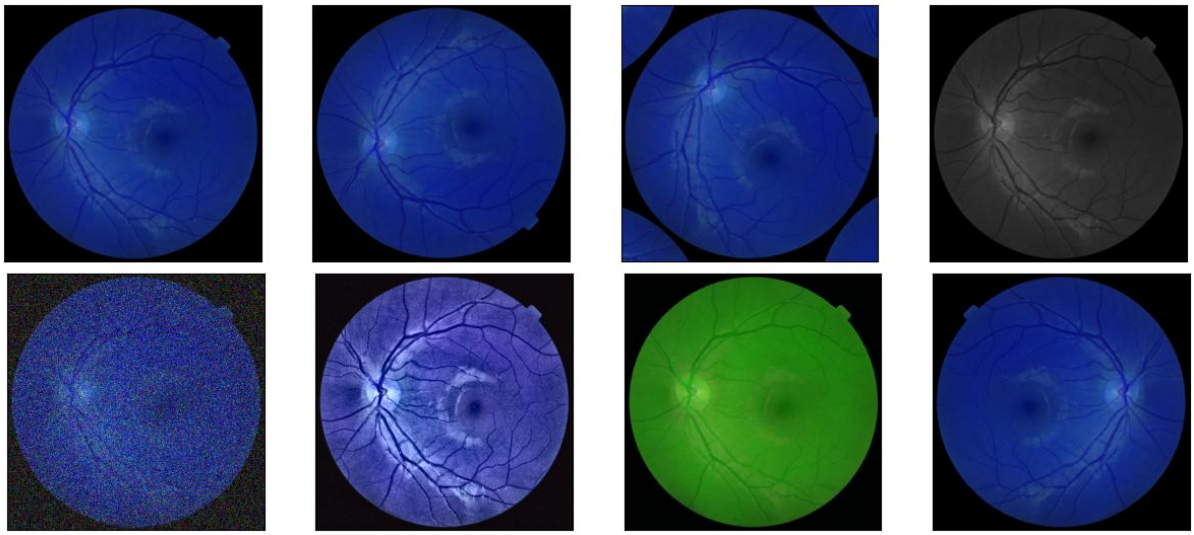

Fig. 11 Augmented Sample Image.

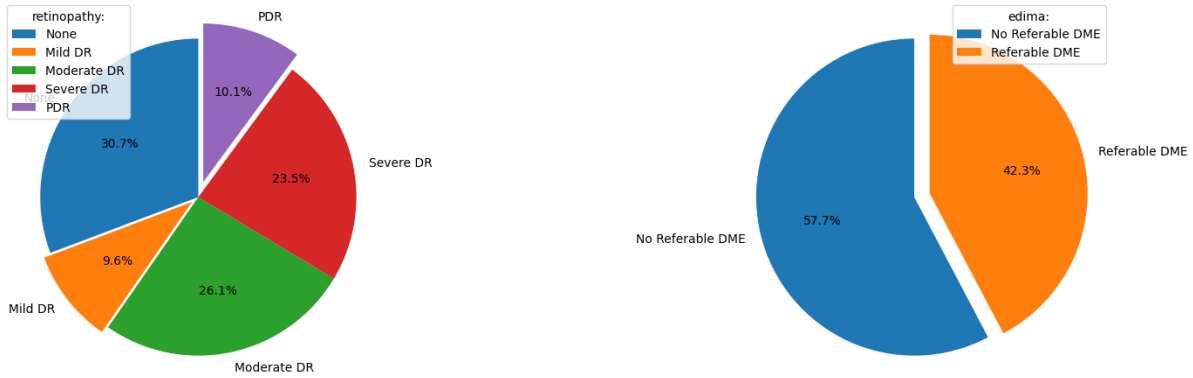

Fig. 12 Retinopathy and Edema after Augmentation.

Table 1 Data Distribution of Retinopathy before and after Data Augmentation.

Augmentation	None	Mild DR	Moderate DR	Severe DR	Proliferative DR	Total
Before	1017	270	347	75	35	1744
After	1017	318	863	777	335	3310

Table 2 Data Distribution of Edema before and after Data Augmentation.

Augmentation	No Referable DME	Referable DME	Total
Before	1593	151	1744
After	1911	1399	3310

4.RESULTS

Python 3 was used to create the suggested method utilizing the Google Colaboratory platform. For the tests, a Windows 10 PC with an Intel i3 processor and 8GB of RAM was utilized. The Convolutional Neural Network (CNN) model achieved 98.86% for Diabetic Macular Edema (DME) and 86.04% for DR during testing. The base model's accuracy is 92.46 for DME and 79.60 for DR. The evaluation's confusion matrix and performance matrix for DME are presented in Tables 4 and 5, respectively, which served as the basis for determining critical performance metrics, such as F-score, accuracy, and precision. Moreover, the performance of the base model Resnet50 and the proposed model has been noted. The results are summarized in Tables 6 and 7 for the performance and confusion matrices of DR. For model implementation, a transfer learning approach using ResNet-50 was employed. The training setup had a learning rate of 0.0003, 100 iterations, and a batch size of 32. To test the performance of the proposed model, several widely used assessment measures were employed, including loss function, optimizer, learning rate, learning rate decay, batch size, epochs, and dropout, as shown in Table 3. The method used to compute these metrics is explained as follows:

$$\textbf{Precision} = \frac{N(TP)}{N(TP)+N(FP)} \quad (1)$$

$$\textbf{Recall} = \frac{N(TP)}{N(TP)+N(FN)} \quad (2)$$

$$\textbf{F-score} = 2 \times \frac{precission * recall}{precission + recall} \quad (3)$$

$$\textbf{Accuracy} = \frac{N(TP)+N(TN)}{N(TP)+N(TN)+N(FP)+N(FN)} \quad (4)$$

5.DISCUSSION

The discussion includes the cumulative counts of true positives (N(TP)), false positives (N(FP)), true negatives (N(TN)), and false negatives (N(FN)), calculated separately for each class. To evaluate the model's overall effectiveness, these values are averaged across the two classes, providing a comprehensive performance measure. The accuracy of the performance analysis is described in the following figures.

Table 3 Represents the Model Hyperparameters and Their Values.

Hyperparameter	Setting
Loss Function	Categorical Cross-Entropy
Optimizer	Adam
Learning Rate	3e-5
Learning Rate Decay	0.3
Batch Size	32
Total number of Batches	104
Epochs	100
Dropout Rate	0.2
Regularization	L2
Early Stopping	No
Validation Set	15% of training samples
Additional Layers	Yes, FC(1024), FC(512), FC(128)
Kernel Size	7 × 7, 3 × 3, 1 × 1
Stride and padding, Pool Size	Stride 2, padding 3, 1, pool 3 × 3, 2 × 2

Table 4 Confusion Matrix for Diabetic Macular Edema.

Model	Proposed		ResNet50 Base	
Class	Predicted		Predicted	
Actual	Abnormal	Normal	Abnormal	Normal
Abnormal	145	3	142	6
Normal	0	117	3	114

Table 5 Performance Matrix in Diabetic Macular Edema Detection and Classification.

Model	Proposed			ResNet50 Base			
Class	Precision	Recall	F1score	Precision	Recall	F1score	Support
Abnormal	1.00	0.98	0.99	0.98	0.96	0.97	148
Normal	0.97	1.00	0.99	0.95	0.97	0.96	117
macro avg	0.99	0.99	0.99	0.96	0.97	0.97	265
weighted avg	0.99	0.99	0.99	0.97	0.97	0.97	265
Accuracy	98.86%			96.60%			

Table 6 Confusion Matrix for 5-class Diabetic Retinopathy for the Proposed Model.

Actual/Predicted		Predicted None	Mild DR	Moderate DR	Severe DR	Proliferative DR
Actual	None	70	2	12	0	0
	Mild DR	2	22	4	0	0
	Moderate DR	11	2	58	0	0
	Severe DR	0	0	3	58	0
	Proliferative DR	0	0	1	0	20

Table 7 Performance Matrix of 5-Class Diabetic Retinopathy for the Proposed Model.

Class	Precision	Recall	F1score	Support	Accuracy (%)	Weighted F1score (%)
None	0.843	0.833	0.838	84		
Mild DR	0.846	0.786	0.815	28		
Moderate DR	0.744	0.817	0.779	71		
Severe DR	1.000	0.951	0.975	61		
Proliferative DR	1.000	0.952	0.975	21		
Macro average	0.887	0.868	0.876	265		
Weighted average	0.865	0.860	0.862	265		
					86.04	86.2

Table 8 Confusion Matrix for 5-Class Diabetic Retinopathy for ResNet50 Base Model.

Actual/Predicted		Predicted None	Mild DR	Moderate DR	Severe DR	Proliferative DR
	None	67	13	3	1	0
	Mild DR	10	13	5	0	0
Actual	Moderate DR	11	4	53	3	0
	Severe DR	0	0	2	59	0
	Proliferative DR	0	1	1	0	19

Table 9 Performance Matrix of 5-Class Diabetic Retinopathy for ResNet50 Base Model.

Class	Precision	Recall	F1score	Support	Accuracy (%)	Weighted F1score(%)
None	0.761	0.798	0.779	84		
Mild DR	0.419	0.464	0.440	28		
Moderate DR	0.828	0.746	0.785	71		
Severe DR	0.937	0.967	0.952	61		
Proliferative DR	1.000	0.905	0.950	21		
Macro average	0.789	0.776	0.781	265		
Weighted average	0.803	0.781	0.788	265		
					79.6	79.8

Table 10 Diabetic Edema Detection and Classification Using External Validation.

Author	DataSet	Classification Model	Accuracy(%)
CNN, Xu et al.	Kaggel	CNN	94.50
Usman et al.	Dataset	ResNet 152	94.40
Alyoubi et al.	Dataset	Resnet 3	85.00
Li, Xiaomeng et al.	IDRiD	ResNet 50	92.60
Pravat et al.	Messidor-2	Modified ResNet 18	95.10
ResNet50 Base	Messidor-2(DME)	ResNet50	92.46
Proposed Model	Messidor-2(DME)	Proposed CNN	98.86
ResNet50 Base	Messidor-2(DR)	ResNet50	79.60
Proposed Model	Messidor-2(DR)	Proposed CNN	86.04

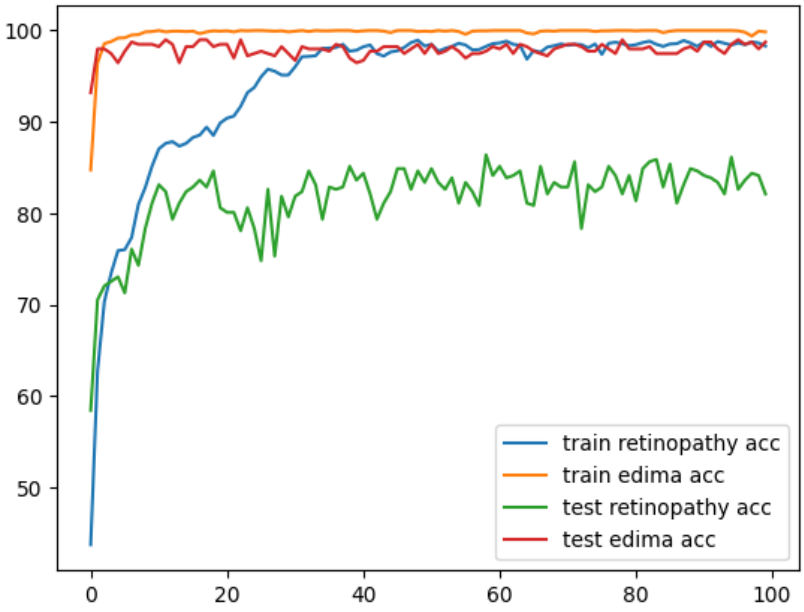

Fig. 11 Retinopathy and Edema Accuracy Graph.

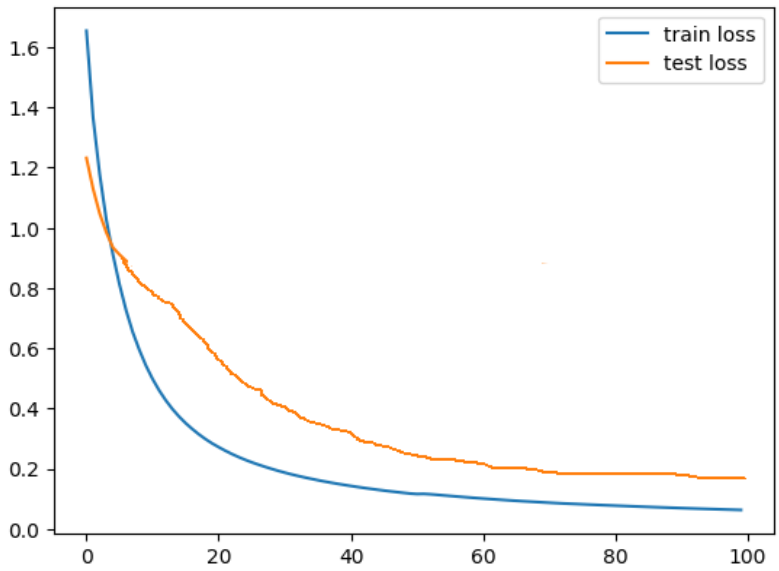

Fig. 12 Representing Train and Test Loss.

6.CONCLUSION

There is a revolutionary opportunity to improve patient outcomes and the standard of care by incorporating Internet of Things (IoT) technologies into the treatment of DR. Clinicians can enhance early diagnosis, ongoing monitoring, and prompt medical intervention for those at risk by employing IoT-enabled devices such as wearable health monitors and retinal imaging devices. Adoption of these technologies, however, also brings up important concerns, such as privacy protection, data security, and system compatibility. Coordinated efforts from patients, regulatory agencies, technology developers, and healthcare professionals are needed to address these issues. The successful implementation of IoT solutions in clinical settings depends on this kind of cooperation. In conclusion, the effectiveness and accessibility of diabetic eye care could be significantly improved by integrating IoT with the treatment of DR.

REFERENCES

[1] Sebastian A, Elharrouss O, Al-Maadeed S, Almaadeed N. **A Survey on Deep-Learning-Based Diabetic Retinopathy Classification**. *Diagnostics* 2023; **13**(3): 345.

[2] Nijalingappa P, Sandeep B. **Machine Learning Approach for the Identification of Diabetes Retinopathy and its Stages**. *Proceedings of the 2015 International Conference on Applied and Theoretical Computing and Communication Technology (iCATccT)* 2015; 653–658.

[3] Raja C, Balaji L. **An Automatic Detection of Blood Vessel in Retinal Images Using Convolution Neural Network for Diabetic Retinopathy Detection**. *Pattern Recognition Image Analysis* 2019; **29**: 533–545.

[4] Vengadapurvaja AM, Nisha G, Aarthy R, Sasikaladevi N. **An Efficient Homomorphic Medical Image Encryption Algorithm for Cloud Storage Security**. *Procedia Computer Science* 2017; **115**: 643-650.

[5] Armknecht F, Boyd C, Carr C, Gjøsteen K, Jäschke A, Reuter CA, Strand M. **A Guide to Fully Homomorphic Encryption**. *Cryptology ePrint Archive* 2015.

[6] Morris L. **Analysis of Partially and Fully Homomorphic Encryption**. *Rochester Institute of Technology* 2013; **10**: 1-5.

[7] Mohanty MD, Das A, Mohanty MN, Altameem A, Nayak SR, Saudagar AKJ, Poonia RC. **Design of Smart and Secured Healthcare Service Using Deep Learning with Modified SHA-256 Algorithm**. *Healthcare* 2022; **10**(7): 1275.

[8] Biswal AK, Singh D, Pattanayak BK, Samanta D, Yang MH. **IoT-Based Smart Alert System for Drowsy Driver Detection**. *Wireless Communications and Mobile Computing* 2021; **2021**: 1-13.

[9] Porwal P, Pachade S, Kamble R, Kokare M, Deshmukh G, Sahasrabuddhe V, Meriaudeau F. **Indian Diabetic Retinopathy Image Dataset (IDRiD): A Database for Diabetic Retinopathy Screening Research**. *Data* 2018; **3**(3): 25.

[10] **(Online Resource/Dataset)**: Omitted. https://www.kaggle.com/datasets/mariaherrerot/messidor2preprocess/data.

[11] Xu K, Feng D, Mi H. **Deep Convolutional Neural Network-Based Early Automated Detection of**

Diabetic Retinopathy Using Fundus Image. *Molecules* 2017; **22**(12): 2054.

[12] Usman TM, Saheed YK, Ignace D, Nsang A. **Diabetic Retinopathy Detection Using Principal Component Analysis Multi-Label Feature Extraction and Classification**. *International Journal of Cognitive Computing in Engineering* 2023; **4**: 78-88.

[13] Alyoubi WL, Shalash WM, Abulkhair MF. **Diabetic Retinopathy Detection Through Deep Learning Techniques: A Review**. *Informatics in Medicine Unlocked* 2020; **20**: 100377.

[14] Li X, Hu X, Yu L, Zhu L, Fu CW, Heng PA. **CANet: Cross-Disease Attention Network for Joint Diabetic Retinopathy and Diabetic Macular Edema Grading**. *IEEE Transactions on Medical Imaging* 2019; **39**(5): 1483-1493.

[15] Abhishek S, Gurrala VR, Sahoo L. **AV Resnet18 Model with Sequential Layer for Computing Accuracy on Image Classification Dataset**. *International Journal of Creative Research Thoughts* 2022; **10**: 2320-2882.

[16] Routray PK, Pattanayak BK, Mohanty MN. **An IoT Application Framework Using Deep Learning for Face Mask Detection**. *Specialusis Ugdymas* 2022; **1**(43): 5450-5464.

[17] Pattanayak BK, Nohur D, Cowlessur SK, Mohanty RK. **An IoT-Based System Architecture for Environmental Monitoring**. *Progress in Advanced Computing and Intelligent Engineering: Proceedings of ICACIE 2020* 2021; 507-514.

[18] Pati A, Parhi M, Pattanayak BK. **IADP: An Integrated Approach for Diabetes Prediction Using Classification Techniques**. *Advances in Distributed Computing and Machine Learning: Proceedings of ICADCML 2021* 2022; 287-298.

[19] Rautaray PK, Pattanayak BK, Mohanty MN, Dash BB, Mohanty B. **Detection of Diabetic Retinopathy Using Multi-Label Feature Extraction and Classification with Fully Homomorphic Encryption**. *South Eastern European Journal of Public Health* 2024; 2564–2576.